Chiral symmetry breaking and the Banks-Casher relation in lattice QCD with Wilson quarks

Leonardo Giusti[a,b] **and Martin Lüscher**[a]

[a] *CERN, Physics Department,*
1211 Geneva 23, Switzerland

[b] *University of Milano-Bicocca and INFN Sezione di Milano-Bicocca,*
Milan, Italy

E-mail: Leonardo.Giusti@cern.ch, Martin.Luescher@cern.ch

ABSTRACT: The Banks-Casher relation links the spontaneous breaking of chiral symmetry in QCD to the presence of a non-zero density of quark modes at the low end of the spectrum of the Dirac operator. Spectral observables like the number of modes in a given energy interval are renormalizable and can therefore be computed using the Wilson formulation of lattice QCD even though the latter violates chiral symmetry at energies on the order of the inverse lattice spacing. Using numerical simulations, we find (in two-flavour QCD) that the low quark modes do condense in the expected way. In particular, the chiral condensate can be accurately calculated simply by counting the low modes on large lattices. Other spectral observables can be considered as well and have a potentially wide range of uses.

Contents

1   Introduction

So far all results obtained in numerical lattice QCD are consistent with the expectation that chiral symmetry is spontaneously broken in the way presumed by chiral perturbation theory. Little is known, however, about the dynamical processes that cause the symmetry to break. An intriguing remark, made long ago by Banks and Casher [1], is that the effect is tied to a condensation of the low modes of the Dirac operator. Studies of the low modes may therefore provide important clues on the symmetry-breaking mechanism.

In the Wilson formulation of lattice QCD [2] and its improved versions [3, 4], chiral symmetry is violated explicitly by terms proportional to the first or second power of the lattice spacing. The Banks-Casher relation consequently cannot be expected to hold exactly and the detailed properties of the low quark modes could be significantly different from those in the continuum theory. On the other hand, as long as only renormalizable quantities are considered, their values in the continuum limit must in principle be computable using the Wilson theory.

The spectral density of the (hermitian) Dirac operator, and thus the average number of quark modes in a given range of eigenvalues, are known to be renormalizable [5]. In the present paper, we first give a second proof of this important fact (section 3). We then discuss the chiral perturbation expansion of the mode numbers and show, in section 5, that their calculation in lattice QCD requires only a modest computational effort. Taken together, these results allow the chiral condensate to be computed in the Wilson theory in a straightforward manner (section 6). Spectral projectors however have a wider range of applicability and provide interesting opportunities to explore the chiral regime of QCD, some of which are briefly mentioned in section 7.

2   Preliminaries

For simplicity we focus on QCD with a doublet of mass-degenerate quarks, but the theoretical discussion is more generally valid and extends to the case of real-world QCD. The quarks will be referred to as the up and down quarks, the associated Goldstone bosons as the pions and the SU(2) flavour symmetry as the isospin symmetry. We consider both the

continuum and the Wilson lattice theory in order to make it clear in which way the mode number computed on the lattice is related to the one defined in the continuum theory.

2.1 Spectral density and mode number in the continuum theory

In a space-time box of volume V with periodic or antiperiodic boundary conditions, the euclidean massless Dirac operator D in presence of a given gauge field has purely imaginary eigenvalues $i\lambda_1$, $i\lambda_2$, ..., which may be ordered so that those with the lower magnitude come first. The associated average spectral density is given by

$$\rho(\lambda, m) = \frac{1}{V} \sum_{k=1}^{\infty} \langle \delta(\lambda - \lambda_k) \rangle \tag{2.1}$$

where the bracket $\langle \ldots \rangle$ denotes the QCD expectation value and m the current-quark mass. Note that the isospin degeneracy is not included in the mode counting, i.e. the Dirac operator is diagonalized in the subspace of, say, the up-quark fields.

The Banks-Casher relation [1]

$$\lim_{\lambda \to 0} \lim_{m \to 0} \lim_{V \to \infty} \rho(\lambda, m) = \frac{\Sigma}{\pi} \tag{2.2}$$

provides a link between the chiral condensate

$$\Sigma = -\lim_{m \to 0} \lim_{V \to \infty} \langle \bar{u}u \rangle \tag{2.3}$$

(where u is the up-quark field) and the spectral density. In particular, if chiral symmetry is spontaneously broken by a non-zero value of the condensate, the density of the quark modes in infinite volume does not vanish at the origin. A non-zero density conversely implies that the symmetry is broken, i.e. the Banks-Casher relation can be read in either direction.

Instead of the spectral density, the average number $\nu(M, m)$ of eigenmodes of the massive hermitian operator $D^\dagger D + m^2$ with eigenvalues $\alpha \leq M^2$ turns out to be a more convenient quantity to consider. Evidently, since

$$\nu(M, m) = V \int_{-\Lambda}^{\Lambda} \mathrm{d}\lambda \, \rho(\lambda, m), \qquad \Lambda = \sqrt{M^2 - m^2}, \tag{2.4}$$

the mode number ultimately carries the same information as the spectral density.

2.2 O(a)-improved lattice QCD

The lattice theory is set up as usual on a hyper-cubic lattice with spacing a, time-like extent T and spatial size L. Periodic boundary conditions are imposed on all fields and in all directions, the only exception being the quark fields which are taken to be antiperiodic in time.

As already mentioned, we focus on the Wilson theory in this paper. The details are not very relevant, but for definiteness we choose the Wilson plaquette action for the gauge field [2] and the standard expression

$$S_{\mathrm{F}} = a^4 \sum_x \left\{ \bar{u}(x) D_m u(x) + \bar{d}(x) D_m d(x) \right\} \tag{2.5}$$

for the quark action, in which D_m denotes the massive, O(a)-improved lattice Dirac operator [3, 4]. Apart from the bare coupling g_0 and the bare mass m_0, the only free parameter in the lattice action is the improvement coefficient c_{sw}, which we choose so as to cancel the O(a) lattice effects in on-shell quantities [6].

In this theory, the renormalized coupling and quark mass are related to the bare parameters through [4]

$$g_{\text{R}}^2 = Z_g(1 + b_g am_{\text{q}})g_0^2, \tag{2.6}$$

$$m_{\text{R}} = Z_m(1 + b_m am_{\text{q}})m_{\text{q}}, \qquad m_{\text{q}} = m_0 - m_{\text{c}}, \tag{2.7}$$

where $m_{\text{c}}(g_0)$ denotes the critical bare mass and $b_g(g_0)$ and $b_m(g_0)$ are further O(a)-improvement coefficients. The renormalization constants Z_g and Z_m depend on the normalization conditions and are functions of the bare coupling and a normalization scale given in units of the lattice spacing.

Composite fields like the isospin axial current and the isospin pseudo-scalar and scalar densities are renormalized similarly by factors of the form $Z_X(1 + b_X am_{\text{q}})$ where $X = A, P, S$. The normalization conditions will be assumed to be such that the renormalized correlation functions satisfy the non-singlet chiral Ward identities up to terms of order a^2. In particular,

$$m_{\text{R}} = \frac{Z_A(1 + b_A am_{\text{q}})}{Z_P(1 + b_P am_{\text{q}})}\, m + \text{O}(a^2), \tag{2.8}$$

where m is the bare current-quark mass that appears in the PCAC relation [4].

On the lattice, we shall be mostly interested in the average number $\nu(M, m_{\text{q}})$ of eigen-modes of $D_m^\dagger D_m$ with eigenvalues $\alpha \leq M^2$. This definition of the mode number formally coincides with the one given in subsection 2.1, but it would evidently be premature to conclude that the values calculated on the lattice are simply related to the mode number defined in the continuum theory.

3 Renormalization of the mode number

The proof of the renormalizability of the mode number given in this section partly follows the lines of ref. [5], but avoids some of the rather technical assumptions that had to be made there. An important new element of the proof is the use of twisted-mass valence quarks and the associated density-chain correlation functions, which have other applications as well (see section 7).

3.1 Spectral sums and density chains

We consider the lattice theory and introduce the spectral sums

$$\sigma_k(\mu, m_{\text{q}}) = \big\langle \text{Tr}\big\{\big(D_m^\dagger D_m + \mu^2\big)^{-k}\big\}\big\rangle, \tag{3.1}$$

where $k \geq 3$ will be assumed for reasons to become clear below. The spectral sums are related to the mode number $\nu(M, m_{\text{q}})$ through the integral transform

$$\sigma_k(\mu, m_{\text{q}}) = \int_0^\infty \text{d}M\, \nu(M, m_{\text{q}})\, \frac{2kM}{(M^2 + \mu^2)^{k+1}}, \tag{3.2}$$
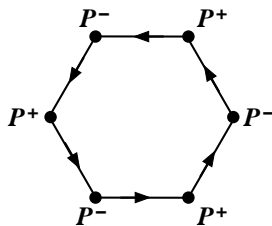
Figure 1. The flavour labels of the pseudo-scalar densities in eq. (3.4) are such that the contraction of the quark fields yields a closed quark loop with six edges. Each edge represents a propagator $(D_m \pm i\mu\gamma_5)^{-1}$ and each vertex contributes a factor γ_5. The ordered product of these factors, summed over the positions $x_1, \ldots, x_6$ of the fields, coincides with the trace (3.1).

which can be shown to be invertible for every fixed k. The renormalization properties of $\nu(M, m_{\mathrm{q}})$ can therefore be inferred from those of, say, $\sigma_3(\mu, m_{\mathrm{q}})$.

The inverse of the operator $D_m^\dagger D_m + \mu^2$ coincides with the square of the quark propagator in twisted-mass lattice QCD [7]. We are thus led to add a set of isospin doublets ψ_l, $l = 1, \ldots, 2k$, of valence-quark fields to the theory, with action

$$S_{\mathrm{F,val}} = a^4 \sum_x \sum_{l=1}^{2k} \overline{\psi}_l(x) \left(D_m + i\mu\gamma_5\tau^3 \right) \psi_l(x) \tag{3.3}$$

(the isospin indices are suppressed in this formula and τ^3 is the third isospin Pauli matrix). Evidently, in order to cancel the valence-quark determinant, a corresponding multiplet of pseudo-fermion fields must be added as well. The spectral sums (3.1) can then be represented by density-chain observables like

$$\sigma_3(\mu, m) = -a^{24} \sum_{x_1, \ldots, x_6} \left\langle P_{12}^+(x_1) P_{23}^-(x_2) P_{34}^+(x_3) P_{45}^-(x_4) P_{56}^+(x_5) P_{61}^-(x_6) \right\rangle, \tag{3.4}$$

where $P_{ij}^\pm = \overline{\psi}_i \gamma_5 \tau^\pm \psi_j$ are the charged pseudo-scalar densities of the valence quarks (see figure 1).

3.2 Renormalization of the spectral sums

With respect to the case of twisted-mass QCD discussed by Frezzotti et al. [7, 8], the $\mathrm{O}(a)$-improvement and renormalization of the partially quenched theory considered here tends to be somewhat simpler. In particular, we may choose a scheme which is independent of the twisted mass parameter and which coincides with the commonly used conventions in the sea-quark sector of the theory.

At $\mu = 0$, the Wilson theory preserves the lattice symmetries, charge conjugation, the gauge symmetry and all (vector) flavour symmetries, including the ones that mix the sea with the valence quarks. Ultraviolet-divergent terms other than those cancelled by the usual parameter and field renormalizations are excluded by these symmetries. When the twisted mass μ is switched on, some of the symmetries are broken and further ultraviolet-divergent terms can arise. Power counting then shows that a multiplicative renormalization,

$$\mu_{\mathrm{R}} = Z_\mu(1 + b_\mu a m_{\mathrm{q}})\mu, \tag{3.5}$$

plus the renormalizations required at $\mu = 0$ are sufficient to renormalize the partially quenched theory. Moreover, the correction proportional to am_q included in eq. (3.5) is all what needs to be added for on-shell O(a)-improvement at $\mu \neq 0$ [8].

Considering eq. (3.4), these remarks suggest that the renormalization of $\sigma_3(\mu, m_q)$ is achieved by multiplication with the sixth power of the renormalization factor Z_P of the pseudo-scalar densities and by renormalizing the parameters of the theory. The only worry one may have at this point is that the summations in eq. (3.4) over the coordinates $x_1, \ldots, x_6$ diverge in the continuum limit. However, as already pointed out in refs. [5, 9, 10], the short-distance singularities of density-chain correlation functions are integrable, and give rise to O(am_q) corrections only, if there are six or more densities.

For any $k \geq 3$, the renormalized O(a)-improved spectral sums are thus given by

$$\sigma_{k,\mathrm{R}}(\mu_\mathrm{R}, m_\mathrm{R}) = \left\{ Z_P \frac{1 + b_P am_q}{1 + b_{PP} am_q} \right\}^{2k} \sigma_k(\mu, m_q), \tag{3.6}$$

where it is understood that the bare masses are expressed through the renormalized ones. The factors $1 + b_{PP} am_q$ in eq. (3.6) are required for the cancellation of the O(am_q) terms alluded to above which derive from the short-distance singularities of the density-chain correlation functions [5].

3.3 Renormalized mode number

If the twisted-mass term is considered to be a perturbation of the theory at $\mu = 0$, one quickly notices that

$$Z_\mu = Z_P^{-1} \tag{3.7}$$

is a possible (and natural) choice of the renormalization factor Z_μ.

Another simplification derives from the identity

$$\frac{\partial}{\partial \mu} \sigma_k(\mu, m_q) = -2k\mu\sigma_{k+1}(\mu, m_q). \tag{3.8}$$

When the renormalized spectral sums are similarly differentiated with respect to the renormalized twisted mass μ_R, the expressions one obtains must be O(a)-improved. As it turns out, this is the case if and only if

$$b_\mu + b_P - b_{PP} = 0. \tag{3.9}$$

The renormalization factor in eq. (3.6) thus becomes

$$Z_P \frac{1 + b_P am_q}{1 + b_{PP} am_q} = \frac{1}{Z_\mu(1 + b_\mu am_q)} \tag{3.10}$$

up to terms of order $a^2 m_q^2$.

Returning to the integral representation (3.2), we now note that the renormalization factor $\{Z_\mu(1 + b_\mu am_q)\}^{-2k}$ needed to renormalize the spectral sum on the left of the equation is cancelled on the right if we substitute

$$M_\mathrm{R} = Z_\mu(1 + b_\mu am_q)M \tag{3.11}$$

and renormalize μ. We are thus led to conclude that

$$\nu_{\mathrm{R}}(M_{\mathrm{R}}, m_{\mathrm{R}}) = \nu(M, m_{\mathrm{q}}) \tag{3.12}$$

is a renormalized and O(a)-improved quantity. In other words, the mode number is a renormalization-group invariant.

3.4 Universality

The steps taken in this section can be repeated using other regularizations of QCD as long as these preserve the same (or more) symmetries as the Wilson theory. Dimensional regularization with the 't Hooft-Veltman prescription for γ_5, for example, has all the required properties, although in this case one is limited to weak-coupling perturbation theory.

Independently of the regularization, the renormalized mode number will be the same if the same normalization conditions are used. In particular, a definite convention such as the $\overline{\mathrm{MS}}$ scheme must be adopted for the normalization of the pseudo-scalar densities. The normalization of the sea-quark mass m_{R} is then determined by the PCAC relation, while the one of μ_{R} is fixed by requiring the identity

$$\frac{\partial}{\partial \mu_{\mathrm{R}}} \sigma_{k,\mathrm{R}}(\mu_{\mathrm{R}}, m_{\mathrm{R}}) = -2k\mu_{\mathrm{R}} \sigma_{k+1,\mathrm{R}}(\mu_{\mathrm{R}}, m_{\mathrm{R}}) \tag{3.13}$$

to hold after removal of the regularization. At this point, the renormalized spectral sums are uniquely determined and so is the renormalized mode number, since the integral transform

$$\sigma_{k,\mathrm{R}}(\mu_{\mathrm{R}}, m_{\mathrm{R}}) = \int_0^\infty \mathrm{d}M_{\mathrm{R}} \, \nu_{\mathrm{R}}(M_{\mathrm{R}}, m_{\mathrm{R}}) \, \frac{2kM_{\mathrm{R}}}{(M_{\mathrm{R}}^2 + \mu_{\mathrm{R}}^2)^{k+1}} \tag{3.14}$$

is free of normalization ambiguities.

4 Chiral expansion of the mode number

In the continuum theory and for small masses, the mode number can be calculated analytically in chiral perturbation theory. Although all results quoted below are for the renormalized mode number, we omit the subscript "R" in this section in order to simplify the notation.

4.1 Chiral perturbation theory

At present the chiral expansion of the spectral density $\rho(\lambda, m)$ is known to next-to-leading order of chiral perturbation theory. The first computation to this order was performed by Smilga and Stern [11] in the massless theory in infinite volume. Later Osborn et al. [12] and Damgaard et al. [13] performed a more complete and systematic computation based on partially quenched chiral perturbation theory [14, 15].

The starting point in the paper of Osborn et al. is the formula

$$\rho(\lambda, m) = \frac{1}{2\pi} \lim_{\epsilon \to 0} \left\{ \Sigma_{\mathrm{val}}(\epsilon + i\lambda) + \Sigma_{\mathrm{val}}(\epsilon - i\lambda) \right\}, \tag{4.1}$$
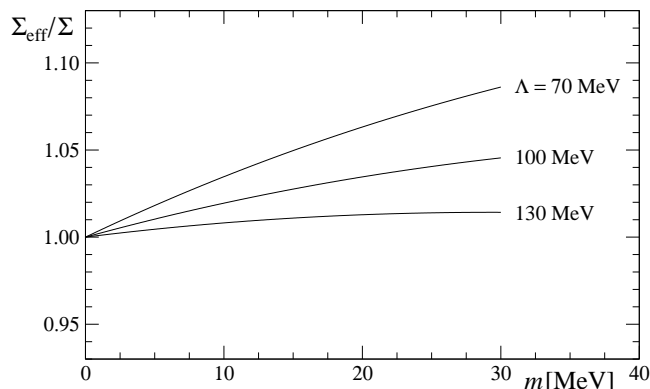
Figure 2. Quark-mass dependence of $\Sigma_{\text{eff}}/\Sigma$ at fixed Λ according to next-to-leading order of chiral perturbation theory. The low-energy constants have been set to $\Sigma = (250\,\text{MeV})^3$, $F = 90\,\text{MeV}$, $\bar{\mu} = 140\,\text{MeV}$ and $\bar{l}_6 = 3$ in this plot.

which relates the spectral density to the expectation value $-\Sigma_{\text{val}}(m_{\text{val}})$ of the scalar density of an added valence quark of mass m_{val}. With a doublet of sea quarks, the relevant graded flavour symmetry group is then SU(3|1) and the chiral expansion of $\Sigma_{\text{val}}(m_{\text{val}})$ is derived from the associated chiral effective theory (see appendix A).

4.2 Large-volume regime

In infinite volume, chiral perturbation theory yields an expansion of $\rho(\lambda, m)$ essentially in powers of λ and m. The leading-order term is given by the Banks-Casher formula and the "effective chiral condensate", defined through

$$\Sigma_{\text{eff}} = \frac{\pi}{2} \frac{\nu(M, m)}{\Lambda V}, \tag{4.2}$$

therefore coincides with Σ in the chiral limit.

At next-to-leading order, the chiral expansion reads

$$\left. \frac{\Sigma_{\text{eff}}}{\Sigma} \right|_{V=\infty} = 1 - \frac{m\Sigma}{16\pi^2 F^4} \left\{ 3 \ln \frac{\Lambda \Sigma}{\bar{\mu}^2 F^2} - 3\bar{l}_6 - 1 + \ln 2 + \ln\left(1 + \frac{m^2}{\Lambda^2}\right) \right.$$
$$\left. + \frac{m}{\Lambda} \arctan \frac{\Lambda}{m} + \frac{\Lambda}{m} \arctan \frac{m}{\Lambda} \right\} + \dots \tag{4.3}$$

The constants F and $\bar{l}_6$ in this expression are, respectively, the pion decay constant in the chiral limit and an SU(3|1) low-energy effective coupling renormalized at scale $\bar{\mu}$ (appendix A). Following the tradition [16], $\bar{\mu}$ may be set to the physical charged-pion mass, but since only the scale-invariant sum of the first two terms in the curly bracket matters, this choice is not compulsory.

A remarkable feature of eq. (4.3) is that the one-loop correction vanishes, for any value of Λ, when the quark mass goes to zero. Smilga and Stern [11] already noted the absence of terms proportional to Λ and showed that this was a special property of the two-flavour theory. The chiral corrections to $\Sigma_{\text{eff}}/\Sigma$ consequently tend to be quite small (see figure 2 for illustration).

4.3 Finite-volume effects

In the present context, the kinematical situation of interest is the so-called p-regime of QCD, where $T \geq L$, $FL \geq 1$ and $m\Sigma V \gg F^2 L^2$. Chiral perturbation theory is easily extended to this regime and can be used to estimate the effects of the finite volume [17].

In the case of Σ_{eff}, the calculation shows that the dependence on the volume sets in at one-loop order and that the infinite-volume limit is reached at an exponential rate according to

$$\Sigma_{\text{eff}} - \Sigma_{\text{eff}}|_{V=\infty} \propto e^{-\frac{1}{2}M_\Lambda L}, \qquad M_\Lambda^2 = \frac{2\Lambda\Sigma}{F^2}. \tag{4.4}$$

Note that M_Λ coincides with the leading-order expression for the mass of a pseudo-scalar meson made of two valence quarks of mass Λ. Since Λ is normally taken to be significantly larger than the sea-quark mass, the finite-size effects (4.4) tend to be smaller than those expected for the pion mass M_π, for example, which decrease like $e^{-M_\pi L}$. In particular, if the parameter values previously used in figure 2 are inserted, and if $L \geq 2\,\text{fm}$ is assumed, Σ_{eff} is estimated to deviate from its infinite-volume value by a fraction of percent at most.

5 Counting the low modes in lattice QCD

In presence of a given gauge field, the number of eigenmodes of $D_m^\dagger D_m$ with eigenvalues $\alpha \leq M^2$ can be determined straightforwardly by calculating the eigenvalues and their multiplicities numerically. The effort required for such computations however grows proportionally to the second or perhaps even a higher power of the space-time volume V. In this section, we show that the modes can be counted more efficiently using spectral projectors.

5.1 Stochastic representation of the mode number

Let $\mathbb{P}_M$ be the orthogonal projector to the subspace of quark fields spanned by the eigenmodes of $D_m^\dagger D_m$ with eigenvalues $\alpha \leq M^2$. An alternative representation of the mode number

$$\nu(M, m_{\text{q}}) = \langle \text{Tr}\{\mathbb{P}_M\} \rangle \tag{5.1}$$

is then given by

$$\nu(M, m_{\text{q}}) = \langle \mathcal{O}_N \rangle, \qquad \mathcal{O}_N = \frac{1}{N} \sum_{k=1}^{N} (\eta_k, \mathbb{P}_M \eta_k), \tag{5.2}$$

where we have added a set of pseudo-fermion fields, $\eta_1, \ldots, \eta_N$, to the theory with action

$$S_\eta = \sum_{k=1}^{N} (\eta_k, \eta_k). \tag{5.3}$$

In the course of a numerical simulation, these fields are generated randomly, for each gauge-field configuration, and the mode number is estimated in the usual way by averaging the observable $\mathcal{O}_N$ over the generated ensemble of fields.

The variance of $\mathcal{O}_N$,

$$\left\langle (\mathcal{O}_N - \langle \mathcal{O}_N \rangle)^2 \right\rangle = \left\langle (\mathrm{Tr}\{\mathbb{P}_M\} - \langle \mathrm{Tr}\{\mathbb{P}_M\} \rangle)^2 \right\rangle + \frac{1}{N} \nu(M, m_{\mathrm{q}}), \qquad (5.4)$$

is larger than the one of $\mathrm{Tr}\{\mathbb{P}_M\}$, but the difference can be reduced by increasing the number N of pseudo-fermion fields. More important may be the fact that the mode number is an extensive quantity, while the variance of $\mathrm{Tr}\{\mathbb{P}_M\}$ does not appear to grow with the volume V of the lattice at the values of M of interest [18]. At fixed N and for a given statistics, the relative statistical error of the calculated mode number is therefore expected to decrease like $V^{-1/2}$.

5.2 Rational approximation

The projector $\mathbb{P}_M$ can be approximated fairly easily by rational functions of $D_m^\dagger D_m$. There are different ways to proceed and the choices made in the following may not be the best ones, but the proposed method is quite efficient and numerically safe.

Let $P(y)$ be the minmax polynomial of degree n which minimizes the deviation

$$\delta = \max_{\epsilon \leq y \leq 1} \left| 1 - \sqrt{y} P(y) \right|. \qquad (5.5)$$

The numerical computation of this polynomial for specified values of n and $\epsilon > 0$ is a standard task in approximation theory (see ref. [19], for example). In the range $-1 \leq x \leq 1$, the function

$$h(x) = \frac{1}{2} \left\{ 1 - x P(x^2) \right\} \qquad (5.6)$$

then provides an approximation to the step function $\theta(-x)$. By construction, the approximation error is at most $\frac{1}{2}\delta$ if $|x| \geq \sqrt{\epsilon}$ and numerical inspection moreover shows that $h(x)$ decreases monotonically in the transition region $|x| \leq \sqrt{\epsilon}$.

An approximation to the projector $\mathbb{P}_M$ is now given by

$$\mathbb{P}_M \simeq h(\mathbb{X})^4, \qquad \mathbb{X} = 1 - \frac{2M_*^2}{D_m^\dagger D_m + M_*^2}, \qquad (5.7)$$

where $M_* \simeq M$ is an adjustable mass parameter. The quality of the approximation is determined by the values of n, ϵ and the ratio M/M_*. In practice, the degree n of the minmax polynomial should be reasonably small and the deviation

$$\Delta = \left\langle \mathrm{Tr}\{\mathbb{P}_M - h(\mathbb{X})^4\} \right\rangle \qquad (5.8)$$

must be much smaller than the statistical errors of the calculated mode numbers.

The estimation of Δ and the choice of M/M_* are discussed in appendix B. Here we only note that the computation of

$$(\eta, \mathbb{P}_M \eta) \simeq (\eta, h(\mathbb{X})^4 \eta) = \|h(\mathbb{X})^2 \eta\|^2 \qquad (5.9)$$

requires the application of the square of $h(\mathbb{X})$ to the pseudo-fermion field η and not of its fourth power.

5.3 Numerical implementation

The minmax polynomial $P(y)$ and therefore the operator $h(\mathbb{X})$ can be expanded in a series of Chebyshev polynomials with rapidly decreasing coefficients [19]. Chebyshev series of this kind can be safely evaluated using the Clenshaw recursion [20].

The computation of $h(\mathbb{X})\eta$ for a given source field η then requires the operator $\mathbb{X}$ to be applied $2n+1$ times. Each application essentially amounts to solving the linear system

$$(D_m^\dagger D_m + M_*^2)\psi = \eta \tag{5.10}$$

using one's favourite iterative algorithm. This system is normally significantly better conditioned than the lattice Dirac equation $D_m\psi = \eta$. Moreover, it is our experience that a fairly loose stopping criterion can be chosen without compromising the correctness of the simulation results.

We finally remark that the computational effort required for the calculation of the mode number along the lines explained here scales like V or at most $V\ln(V)$ as the lattice is increased.

6 Computation of the chiral condensate

The simulations discussed in this section have a limited scope, but the results clearly show that the low modes of the Dirac operator condense and that the mode number can be accurately computed using the stochastic method described in the previous section.

We have considered two lattices in these studies, with spacing $a \simeq 0.08\,\mathrm{fm}$, spatial sizes $L \simeq 1.9\,\mathrm{fm}$ and $2.5\,\mathrm{fm}$, respectively, and time-like extents $T = 2L$. The exact parameter values and further technical details are given in appendix C. All values quoted for the renormalized mass parameters, the mass-dependent condensate $\overline{\Sigma}_\mathrm{R}$ defined in subsection 6.3 and the condensate Σ refer to the $\overline{\mathrm{MS}}$ scheme at $2\,\mathrm{GeV}$.

6.1 Qualitative behaviour of the mode number

The data plotted in figure 3 show that the mode number is, in the case considered, a nearly linear function of M_R from above the threshold region at $M_\mathrm{R} \simeq m_\mathrm{R}$ up to at least $110\,\mathrm{MeV}$. This behaviour is qualitatively in line with chiral perturbation theory, but the fact that the linear regime extends to such large values of M_R is rather striking and could not be foreseen.

At the very low end of the spectrum, the curve shown in figure 3 however clearly deviates from its expected form in the continuum theory (shaded area in figure 3) [5]. A plausible explanation of the observed deviation is that chiral symmetry is not exactly preserved in the Wilson theory and that the fine structure of the spectrum of the Dirac operator near the threshold at $M_\mathrm{R} = m_\mathrm{R}$ is consequently not protected from perturbing lattice effects [21]. The deviation must in any case be a lattice artefact, since the renormalized mode number is bound to converge to its continuum value as the lattice spacing is decreased (cf. section 3).

In the following, we focus on the linear regime in figure 3, where the mode number is not expected to be particularly sensitive to discretisation errors. Moreover, since the
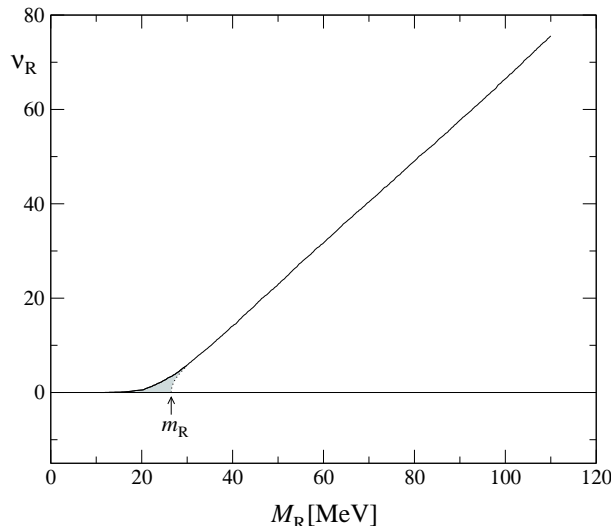
Figure 3. Dependence of the renormalized mode number on M_R at $m_R \simeq 26\,\text{MeV}$ and $L \simeq 2.5\,\text{fm}$. The curve shown is based on a representative ensemble of 71 gauge-field configurations and required the lowest 80 eigenvalues of $D_m^\dagger D_m$ to be calculated for each of these fields. Statistical errors are slightly larger than the jitter of the curve.

effort required for the numerical calculation of the low eigenvalues of $D_m^\dagger D_m$ is not small, the mode number was normally computed using the method described in section 5 and we shall, from now on, only discuss results obtained in this way.

6.2 Volume-dependence of the mode number

In the large-volume regime of the theory, $\nu(M, m_q)/V$ is expected to be independent of the lattice size up to exponentially small corrections (cf. section 4). The lattices we have simulated are such that we can immediately check whether these corrections are significant at the level of the statistical errors.

To this end, we form the ratios

$$r_{3,4} = \frac{\nu(M, m_q)_{D_3}}{\nu(M, m_q)_{E_4}} \left(\frac{32}{24}\right)^4, \qquad r_{5,5} = \frac{\nu(M, m_q)_{D_5}}{\nu(M, m_q)_{E_5}} \left(\frac{32}{24}\right)^4, \tag{6.1}$$

where the subscripts D_3 etc. refer to the run label quoted in table 2 (appendix C). Both ratios turn out to be practically equal to 1. More precisely, $r_{3,4}$ differs from 1 by -0.6 to -2.0 standard deviations and $r_{5,5}$ by $+0.7$ to $+1.5$ standard deviations as M varies over the values listed in table 2. There are thus no indications for significant finite-volume effects on these lattices.

6.3 Calculation of Σ

The values of the renormalized mode number which we calculated on the larger of the two lattices considered are plotted in figure 4 (left graph). At fixed quark mass, the mode number is, to a very good approximation, a linear function of M_R in the range shown
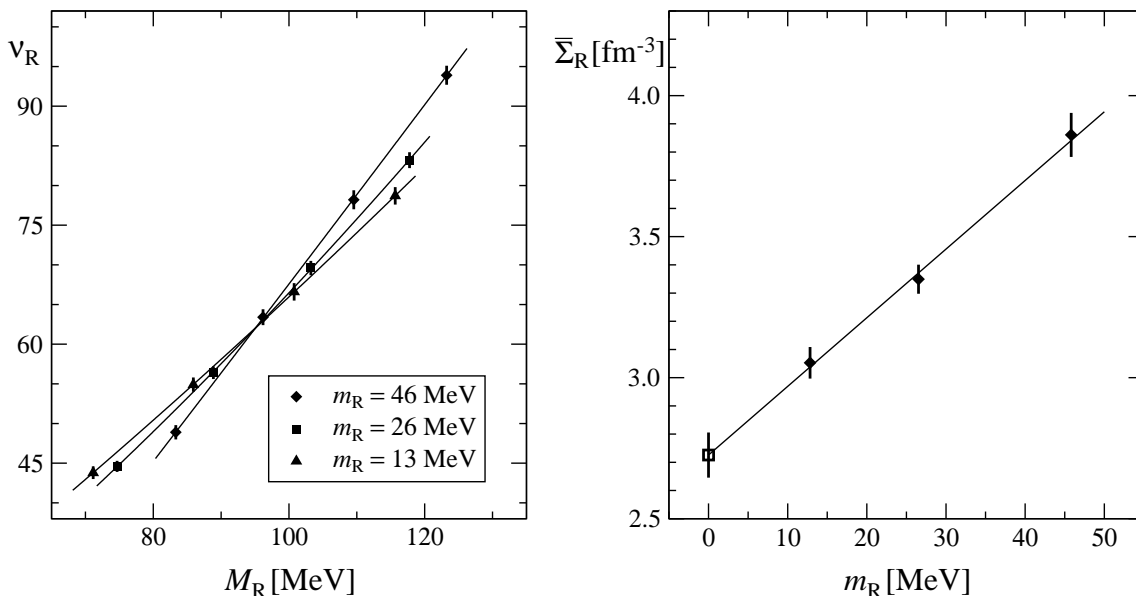
Figure 4. Simulation results for the renormalized mode number at fixed $L \simeq 2.5\,\mathrm{fm}$ (plot on the left). The linear extrapolation to the chiral limit (open square) of $\overline{\Sigma}_{\mathrm{R}}$ at $M_{\mathrm{R}} = 95\,\mathrm{MeV}$ is shown on the right. All errors in these plots are statistical only.

in the figure. In particular, the slope of the data can easily be determined by quadratic interpolation (lines in the left graph).

We are thus led to introduce the mass-dependent condensate

$$\overline{\Sigma}_{\mathrm{R}} = \frac{\pi}{2V} \sqrt{1 - \left(\frac{m_{\mathrm{R}}}{M_{\mathrm{R}}}\right)^2} \frac{\partial}{\partial M_{\mathrm{R}}} \nu_{\mathrm{R}}(M_{\mathrm{R}}, m_{\mathrm{R}}), \tag{6.2}$$

where the prefactor is chosen such that $\overline{\Sigma}_{\mathrm{R}}$ coincides with the chiral condensate Σ to leading order of chiral perturbation theory. In table 1 we list the calculated values of $\overline{\Sigma}_{\mathrm{R}}$ at $M_{\mathrm{R}} = 95\,\mathrm{MeV}$ (a point in the middle of the available range of masses). The first errors quoted in the table are the statistical ones, while the second errors are those inherited from the product of the lattice spacing and the renormalization factors needed to convert from lattice to physical normalizations (appendix C).

The next-to-leading order formula (4.3) suggests that $\overline{\Sigma}_{\mathrm{R}} = \Sigma$ up to higher-order corrections and terms vanishing proportionally to m_{R} in the chiral limit. Note that there are no terms proportional to $m_{\mathrm{R}} \ln m_{\mathrm{R}}$ at this order of the chiral expansion. The data for $\overline{\Sigma}_{\mathrm{R}}$ at $M_{\mathrm{R}} = 95\,\mathrm{MeV}$ actually fall on a straight line (right graph in figure 4) and the extrapolation to $m_{\mathrm{R}} = 0$ then yields the estimate

$$\Sigma^{1/3} = 276(3)(4)(5)\,\mathrm{MeV} \tag{6.3}$$

for the chiral condensate. Higher-order corrections were neglected here, but appear to be small as the results vary only little (within roughly the third error given above) when the chiral limit is taken at other values of M_{R}.

Run	m_{R} [MeV]	$\overline{\Sigma}_{\mathrm{R}}^{1/3}$ [MeV]
E_4	45.8(3)(11)	310(2)(4)
E_5	26.5(2)(6)	295(2)(4)
E_6	12.8(2)(3)	286(2)(4)

Table 1. Simulation results for $\overline{\Sigma}_{\mathrm{R}}$ at $M_{\mathrm{R}} = 95\,\mathrm{MeV}$

It goes without saying, however, that this procedure and the quoted result for the condensate will have to be confirmed by more extensive calculations. Meanwhile we note that the estimate (6.3) is in the range of values obtained in two- and three-flavour QCD from chiral fits of the quark-mass dependence of the pion mass [22]–[24] and from studies of the so-called ϵ-regime of QCD [25]–[29].

7 Further uses of spectral observables

Spectral observables like the mode number provide interesting probes of low-energy QCD. In this section we wish to show that the computation of the chiral condensate is only one of the possible applications of these observables.

7.1 Scaling to the continuum limit

Extrapolations to the continuum limit require simulations of a series of lattices with decreasing lattice spacings. Since only the bare coupling and bare quark mass can be prescribed, the ratios of the spacings of the simulated lattices are not known a priori and need to be calculated. Evidently, it is very important to obtain the ratios with small statistical and systematic errors.

A set of O(a)-improved renormalized quantities, which may conceivably be used to match the lattices, is[1]

$$\left\{ M_\pi, M_{\mathrm{R}} G_{\pi,\mathrm{R}}, \frac{\nu_{\mathrm{R}}}{V} \right\}, \tag{7.1}$$

where M_π and $G_{\pi,\mathrm{R}}$ are, respectively, the pion mass and the renormalized vacuum-to-pion matrix element of the isospin pseudo-scalar density. All these quantities are renormalization-group invariants. In particular, the dimensionless combinations

$$C_1 = M_\pi^2 \left(\frac{V}{\nu_{\mathrm{R}}} \right)^{1/2}, \tag{7.2}$$

$$C_2 = (M_{\mathrm{R}} G_{\pi,\mathrm{R}})^4 \left(\frac{V}{\nu_{\mathrm{R}}} \right)^3, \tag{7.3}$$

are well-defined and directly accessible functions of g_0, am_0 and aM.

Since C_1 and C_2 are roughly linearly rising with am_0 and aM, respectively, it is possible to match the mass parameters on any given pair of lattices by requiring C_1 and

---

[1]The list of observables given here only serves to illustrate the general ideas. In particular, the combination $M_{\mathrm{R}} \overline{\Sigma}_{\mathrm{R}}$ may be used in place of ν_{R}/V.

C_2 to assume the same (sensibly chosen) values. After that the ratio of the lattice spacings is obtained through

$$\frac{a_1}{a_2} = \left(\frac{\nu_1 n_2}{n_1 \nu_2}\right)^{1/4}, \tag{7.4}$$

where n_1, n_2 denote the numbers of points of the two lattices and ν_1, ν_2 the mode numbers at the matched values of the mass parameters (we implicitly assumed here that finite-volume effects can be neglected or that the volumes are the same).

An important technical advantage of this procedure is that all quantities involved are easily obtained with small errors. In particular, the statistical precision that can be attained in practice is not expected to change dramatically as the lattice spacing is decreased or if larger lattices are considered.

7.2 Computation of renormalization constants

Density-chain correlation functions like the ones discussed in section 3 satisfy various chiral Ward identities in the continuum limit. We may, for example, start from the "twisted spectral sums"

$$\sigma_{k,l}(\mu, m_{\mathrm{q}}) = \left\langle \mathrm{Tr}\left\{\gamma_5 \left(D_m^\dagger D_m + \mu^2\right)^{-k} \gamma_5 \left(D_m^\dagger D_m + \mu^2\right)^{-l}\right\}\right\rangle, \tag{7.5}$$

which can be represented through density-chain correlation functions of the form

$$\sigma_{1,2}(\mu, m_{\mathrm{q}}) = -a^{24} \sum_{x_1,\ldots,x_6} \left\langle S_{12}^+(x_1) P_{23}^-(x_2) S_{34}^+(x_3) P_{45}^-(x_4) P_{56}^+(x_5) P_{61}^-(x_6)\right\rangle. \tag{7.6}$$

In the continuum limit and if $k + l \geq 3$, chiral symmetry (or simply the fact that γ_5 commutes with $D_m^\dagger D_m$ in the continuum theory) then implies that the properly renormalized twisted spectral sum $\sigma_{k,l,\mathrm{R}}$ coincides with $\sigma_{k+l,\mathrm{R}}$.

On the lattice one should keep track of the O(a) corrections, but following the lines of ref. [5], it is then straightforward to show that

$$\frac{Z_P^2}{Z_S^2} = (1 + 2b_R a m_{\mathrm{q}}) \frac{\sigma_{k,l}}{\sigma_{k+l}} + \mathrm{O}(a^2), \tag{7.7}$$

$$b_R = b_S - b_P + 2(b_{PP} - b_{PS}), \tag{7.8}$$

where the improvement coefficient b_R is known to one-loop order of perturbation theory and appears to be small (appendix C).

Equation (7.7) is actually a special case of a more general Ward identity, where the inverse powers of $D_m^\dagger D_m + \mu^2$ in the definition of the spectral sums are replaced by any sufficiently rapidly decaying functions of $D_m^\dagger D_m$. In particular,

$$\frac{Z_P^2}{Z_S^2} = (1 + 2b_R a m_{\mathrm{q}}) \frac{\langle \mathrm{Tr}\{\gamma_5 \mathbb{P}_M \gamma_5 \mathbb{P}_M\}\rangle}{\langle \mathrm{Tr}\{\mathbb{P}_M\}\rangle} + \mathrm{O}(a^2) \tag{7.9}$$

is an identity recommended for numerical evaluation.

7.3 Topological susceptibility

Using parity-odd density chains, the topological susceptibility χ_t in QCD can be defined in a manifestly ultraviolet-finite and therefore universally valid way [10]. On the lattice there exist different definitions of this type, all of which are expected to coincide in the continuum limit. In particular, one can make use of twisted-mass density chains and it is then possible, as in the case of the chiral Ward identities discussed in the previous subsection, to pass from density chains to spectral projectors.

Proceeding along these lines, the expression

$$\chi_t = (1 + 2b_R a m_{\rm q}) \frac{Z_S^2}{Z_P^2} \frac{1}{V} \langle {\rm Tr}\{\gamma_5 \mathbb{P}_M\} {\rm Tr}\{\gamma_5 \mathbb{P}_M\} \rangle + {\rm O}(a^2) \tag{7.10}$$

is obtained, which, when combined with eq. (7.9), leads to the formula

$$\chi_t = \frac{\nu}{V} \frac{\langle {\rm Tr}\{\gamma_5 \mathbb{P}_M\} {\rm Tr}\{\gamma_5 \mathbb{P}_M\} \rangle}{\langle {\rm Tr}\{\gamma_5 \mathbb{P}_M \gamma_5 \mathbb{P}_M\} \rangle} + {\rm O}(a^2). \tag{7.11}$$

In principle the mass $M_{\rm R}$ can be set to any value in eqs. (7.9)–(7.11), but since the size of the lattice effects depends on $M_{\rm R}$, its value should in practice be chosen with some care. One evidently requires that $aM_{\rm R} \ll 1$ and it is certainly wise to avoid the threshold region $M_{\rm R} \simeq m_{\rm R}$, where the lattice effects tend to be kinematically enhanced. Moreover, a definite prescription that fixes $M_{\rm R}$ in physical units should be adopted when scaling to the continuum limit, as otherwise there is no guarantee that the calculated renormalized quantities converge with a rate proportional to a^2.

8 Concluding remarks

The condensation of the low modes of the Dirac operator seen in numerical lattice QCD provides a most direct piece of theoretical evidence for the spontaneous breaking of chiral symmetry in QCD. Explicit violations of chiral symmetry at momenta on the order of the inverse lattice spacing have little influence on the mode condensation, because the mode number is a renormalizable quantity and therefore coincides with its continuum limit up to terms that vanish proportionally to a power of the lattice spacing.

The dynamical mechanisms that cause the modes to condense are presently not known. It is quite clear, however, that the spontaneous breaking of chiral symmetry is not a many-quark collective effect. The mode condensation actually appears to be largely insensitive to the sea-quark mass and it seems to persist even when passing to the quenched theory. There is thus no relevant back-reaction of the sea quarks and theoretical studies of the behaviour of a single quark in presence of representative gauge fields may therefore allow the breaking of chiral symmetry to be explained.

While the computation of the chiral condensate is an obvious application of the spectral projector technique introduced in this paper, there are other applications as well and the technique is also not limited to a particular lattice formulation of QCD. Moreover, it may be useful for studies of the theory at non-zero temperature and of QCD-like theories, where chiral symmetry may or may not be spontaneously broken.

A SU(3|1) chiral perturbation theory

As explained in section 4, the chiral expansion of the spectral density (and thus of the mode number) is obtained by calculating the valence-quark condensate $\Sigma_{\mathrm{val}}(m_{\mathrm{val}})$ in partially quenched chiral perturbation theory [14, 15]. We here provide some details of this computation, assuming the reader is familiar with chiral perturbation theory and partial quenching.

Following a suggestion of Sharpe and Shoresh [15], we do not include a flavour-singlet field in the effective chiral theory. In the sea-quark sector, the chiral expansions generated by the SU(3|1) chiral lagrangian then literally coincide with those obtained in the standard SU(2) theory. In particular, the low-energy constants (such as F and Σ) which already occur in the latter are the same.

A.1 Group generators

The complex Lie superalgebra of SU(3|1) consists of all 4×4 supermatrices $X_{\alpha\beta}$ with vanishing supertrace (see ref. [30], for example). We assume the indices α, β of these matrices to be such that $\alpha = 1, 2$ corresponds to the sea quarks, $\alpha = 3$ to the valence quark and $\alpha = 4$ to the ghost (or pseudo-fermion) quark associated to the valence quark.

Our conventions for the generators T^a, $a = 1, \ldots, 15$, of the algebra are

$$T^a = (T^a)^\dagger, \qquad \mathrm{Str}\{T^a\} = 0, \qquad \mathrm{Str}\{T^a T^b\} = \frac{1}{2} g^{ab}, \tag{A.1}$$

where the non-zero elements of the matrix g^{ab} are given by

$$g = \begin{pmatrix} 1 & \ddots & & & & \\ & 1 & & & & \\ & & -\tau^2 & & & \\ & & & \ddots & & \\ & & & & -\tau^2 & \\ & & & & & -1 \end{pmatrix} \begin{matrix} \left.\vphantom{\begin{matrix}1\\1\end{matrix}}\right\} & 1-8 \\ \\ \left.\vphantom{\begin{matrix}1\\1\end{matrix}}\right\} & 9-14 \\ \\ \left.\vphantom{1}\right\} & 15 \end{matrix} \tag{A.2}$$

More specifically, $T^1, \ldots, T^8$ are assumed to be generators of the SU(3) subgroup acting on the sea and valence quarks, while $T^9, \ldots, T^{14}$ mix the ghost with the other quarks and T^{15} is a diagonal matrix with a non-zero ghost-quark component.

In the following the Einstein summation convention is adopted for SU(3|1) group indices and for Lorentz indices. It is also helpful to introduce the tensors

$$h^{ab} = (g^{a8} - g^{a15})(g^{b8} - g^{b15}), \qquad k^{ab} = (g^{a8} + g^{a15})(g^{b8} + g^{b15}), \tag{A.3}$$

which satisfy $k^{ac} h^{cb} = 0$.

A.2 Chiral effective lagrangian

The $SU(3|1)$ chiral effective theory is a non-linear σ-model in which the basic field $U(x)$ takes values in $SU(3|1)$. As usual the lagrangian

$$\mathcal{L} = \mathcal{L}^{(2)} + \mathcal{L}^{(4)} + \dots \tag{A.4}$$

is given as a series of terms of increasing dimension. The leading-order term,

$$\mathcal{L}^{(2)} = -\frac{1}{4}F^2\,\mathrm{Str}\{J_\mu J_\mu\} - \frac{1}{2}BF^2\,\mathrm{Str}\{MU^\dagger + M^\dagger U\}, \qquad J_\mu = U^\dagger \partial_\mu U, \tag{A.5}$$

involves the quark mass matrix M, the pion decay constant in the chiral limit, F, and the parameter B, which is related to the quark condensate through $\Sigma = BF^2$. The mass matrix is taken to be diagonal,

$$M = \mathrm{diag}\{m, m, m_{\mathrm{val}}, \tilde{m}_{\mathrm{val}}\}, \tag{A.6}$$

where m, m_{val} and $\tilde{m}_{\mathrm{val}}$ are, respectively, the masses of the sea quarks, the valence quark and the ghost quark. In order to properly quench the valence quark, $\tilde{m}_{\mathrm{val}}$ will later be set to m_{val}.

At next-to-leading order, the effective lagrangian reads

$$\mathcal{L}^{(4)} = -L_0\mathrm{Str}\{J_\mu J_\nu J_\mu J_\nu\} - \left(L_1 - \frac{1}{2}L_0\right)\mathrm{Str}\{J_\mu J_\mu\}\mathrm{Str}\{J_\nu J_\nu\} \tag{A.7}$$

$$-(L_2 - L_0)\mathrm{Str}\{J_\mu J_\nu\}\mathrm{Str}\{J_\mu J_\nu\} - (L_3 + 2L_0)\mathrm{Str}\{J_\mu J_\mu J_\nu J_\nu\}$$

$$-2BL_4\mathrm{Str}\{J_\mu J_\mu\}\mathrm{Str}\{MU^\dagger + M^\dagger U\} - 2BL_5\mathrm{Str}\{J_\mu J_\mu(U^\dagger M + M^\dagger U)\}$$

$$-4B^2L_6\mathrm{Str}\{U^\dagger M + M^\dagger U\}\mathrm{Str}\{U^\dagger M + M^\dagger U\}$$

$$-4B^2L_7\mathrm{Str}\{M^\dagger U - MU^\dagger\}\mathrm{Str}\{M^\dagger U - MU^\dagger\}$$

$$-4B^2L_8\mathrm{Str}\{MU^\dagger MU^\dagger + M^\dagger UM^\dagger U\} - 4B^2H_2\mathrm{Str}\{M^\dagger M\}.$$

The additional low-energy constants at this order are thus $L_0, \dots, L_8$ and H_2. Note that in these expressions we have omitted all terms that do not contribute to the valence-quark condensate (such as those related to current correlation functions, for example) [16].

A.3 Perturbation expansion

The chiral expansion of

$$\Sigma_{\mathrm{val}}(m_{\mathrm{val}}) = -\langle\sigma_{\mathrm{val}}\rangle_{\tilde{m}_{\mathrm{val}}=m_{\mathrm{val}}}, \tag{A.8}$$

$$\sigma_{\mathrm{val}} = \frac{\partial\mathcal{L}}{\partial m_{\mathrm{val}}} = -\Sigma\,\mathrm{Re}\,U_{33} + \dots, \tag{A.9}$$

is obtained by substituting

$$U = \exp\{2i\phi/F\}, \qquad \phi = \phi^a T^a, \tag{A.10}$$

in the functional integral and expanding all entries in powers of ϕ. Since the expectation value in eq. (A.8) is to be computed at $\tilde{m}_{\text{val}} = m_{\text{val}}$, one needs to work out the Feynman rules only for this case.

To second order in ϕ, the leading-order lagrangian reads

$$\mathcal{L}^{(2)} = \frac{1}{2} g^{ab} \{ \partial_\mu \phi^a \partial_\mu \phi^b + M_a^2 \phi^a \phi^b \} + \frac{1}{6} (M_{\text{ss}}^2 - M_{\text{vv}}^2) k^{ab} \phi^a \phi^b, \tag{A.11}$$

where $M_{\text{ss}}^2 = 2Bm$, $M_{\text{vv}}^2 = 2Bm_{\text{val}}$ and

$$M_a^2 = \begin{cases} M_{\text{ss}}^2 & \text{if a=1,2,3,} \\ \frac{1}{2}(M_{\text{ss}}^2 + M_{\text{vv}}^2) & \text{if a=4,\dots,7,9,\dots,12,} \\ M_{\text{vv}}^2 & \text{if a=8,13,14,15.} \end{cases} \tag{A.12}$$

The propagator of the meson field is thus given by

$$\langle \phi^a(x) \phi^b(0) \rangle = g^{ab} G_1(x, M_a^2) + \frac{1}{3} (M_{\text{vv}}^2 - M_{\text{ss}}^2) h^{ab} G_2(x, M_a^2), \tag{A.13}$$

$$G_n(x, M^2) = \int \frac{\mathrm{d}^4 p}{(2\pi)^4} \frac{\mathrm{e}^{ipx}}{(p^2 + M^2)^n}. \tag{A.14}$$

All other Feynman rules can be derived straightforwardly from the lagrangian and the field σ_{val}.

Following common practice, we use dimensional regularization for the loop integrals and a modified minimal subtraction scheme for the bare couplings in the lagrangian $\mathcal{L}^{(4)}$. In particular, in $4 - 2\epsilon$ dimensions we substitute

$$L_6 = \frac{3\bar{\mu}^{-2\epsilon}}{(32\pi)^2} \left\{ -\frac{1}{\epsilon} + \gamma - \ln 4\pi - 1 + \bar{l}_6 \right\} \tag{A.15}$$

for the coupling L_6, where $\gamma = 0.577\ldots$ denotes Euler's constant, $\bar{l}_6$ the renormalized coupling and $\bar{\mu}$ the renormalization scale.
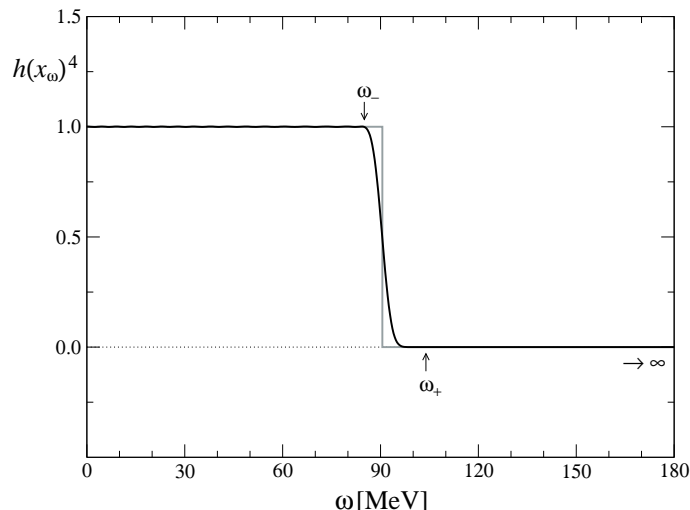
A.4 Finite-volume correction

The chiral expansion

$$\Sigma_{\text{val}}(m_{\text{val}}) - \Sigma_{\text{val}}(m_{\text{val}})|_{V=\infty} = \frac{\Sigma}{2F^2} \bigg\{ g_1(M_{\text{vv}}^2) - 4g_1\left(\frac{1}{2}M_{\text{ss}}^2 + \frac{1}{2}M_{\text{vv}}^2\right) \tag{A.16}$$
$$+ (M_{\text{ss}}^2 - M_{\text{vv}}^2) \, g_2(M_{\text{vv}}^2) \bigg\} + \ldots$$

starts at next-to-leading order and involves the momentum sums

$$g_n(M^2) = \frac{1}{V} \sum_p \frac{1}{(p^2 + M^2)^n} - G_n(0, M^2). \tag{A.17}$$

These are easily calculated numerically when written in the form of rapidly converging series of Bessel functions [17].

Figure 5. Approximate spectral step function $h(x_\omega)^4$ for $n = 32$, $\epsilon = 0.01$ and $M_* = 94\,\mathrm{MeV}$. The exact step function $\theta(M - \omega)$ is also shown (grey line), where M and M_* are related through eq. (B.7).

B   Estimation of the approximation error Δ

The computational strategy outlined in section 5 assumes that the parameters n, ϵ, M and M_* are such that the approximation error Δ [eq. (5.8)] can be safely neglected. In this appendix, we now show how this condition can be met in practice.

B.1   Spectral integral

Our starting point is the spectral integral representation

$$\Delta = \int_0^\infty \mathrm{d}\omega \left\{ \theta(M - \omega) - h(x_\omega)^4 \right\} \nu'(\omega, m_\mathrm{q}) \tag{B.1}$$

in which

$$\nu'(\omega, m_\mathrm{q}) = \frac{\partial}{\partial \omega} \nu(\omega, m_\mathrm{q}), \qquad x_\omega = 1 - \frac{2M_*^2}{\omega^2 + M_*^2}. \tag{B.2}$$

Note that $\nu'(\omega, m_\mathrm{q})$ coincides with the average spectral density of the square root of $D_m^\dagger D_m$ up to a factor V. For illustration, the two functions in the curly bracket are plotted in figure 5 for a typical choice of the parameters.

In the following, we distinguish three ranges of ω, separated by the limits

$$\omega_\pm = M_* \left(\frac{1 \pm \sqrt{\epsilon}}{1 \mp \sqrt{\epsilon}} \right)^{1/2} \tag{B.3}$$

of the transition region around $\omega = M_*$ (see figure 5). The parts of the spectral integral corresponding to the integration ranges $[0, \omega_-]$, $[\omega_-, \omega_+]$ and $[\omega_+, \infty]$ are denoted by Δ_-, Δ_0 and Δ_+, respectively.

B.2 Bounds on Δ_+ and Δ_-

Noting

$$x_\omega = \pm\sqrt{\epsilon} \quad \text{at} \quad \omega = \omega_\pm \tag{B.4}$$

and recalling the approximation property (5.5) of the minmax polynomial $P(y)$, the function in the curly bracket in eq. (B.1) is easily bounded in the case of the integrals $\Delta_\pm$. Since the total number of eigenmodes of $D_m^\dagger D_m$ is $12V/a^4$ and since there are at most $\nu(M, m_q)$ eigenmodes with eigenvalues $\omega^2 \leq \omega_-^2$, it is then straightforward to establish the bounds

$$|\Delta_+| \leq \frac{3}{4} \frac{V\delta^4}{a^4}, \tag{B.5}$$

$$|\Delta_-| \leq \nu(M, m_q) \left\{ 2\delta + O(\delta^2) \right\}. \tag{B.6}$$

These parts of the total error Δ are thus controlled by the precision δ of the polynomial approximation to the step function.

In ref. [19] it was shown that δ is an exponentially decreasing function of $n\sqrt{\epsilon}$. The precision can therefore be set to the desired level by adjusting the degree n of the minmax polynomial. If $\epsilon = 0.01$, for example, and if a lattice of size 128×64^3 is considered, a sensible choice is $n = 32$ and eqs. (B.5), (B.6) then imply that $|\Delta_+| \leq 10^{-6}$ and $|\Delta_-| \leq 10^{-3} \times \nu(M, m_q)$.

B.3 Estimation of Δ_0 and the relation of M to M_*

The remaining error component, Δ_0, is more difficult to estimate than Δ_+ and Δ_-. An important point to note is that the density $\nu'(\omega, m_q)$ tends to be practically constant in the transition region (cf. section 6). Most of the error can therefore be cancelled by choosing the relation between M and M_* to be such that Δ_0 vanishes for a constant density. This condition amounts to setting

$$\frac{M}{M_*} = \left(\frac{1 - \sqrt{\epsilon}}{1 + \sqrt{\epsilon}} \right)^{1/2} + \int_{-\sqrt{\epsilon}}^{\sqrt{\epsilon}} dx \, \frac{1 + x}{(1 - x^2)^{3/2}} \, h(x)^4 \tag{B.7}$$

and the residual value of the error,

$$\Delta_0 = \int_{\omega_-}^{\omega_+} d\omega \left\{ \theta(M - \omega) - h(x_\omega)^4 \right\} \left\{ \nu'(\omega, m_q) - \nu'(M, m_q) \right\}, \tag{B.8}$$

is then of order ϵ.

An estimation of Δ_0 however requires some information on the ω-dependence of the density $\nu'(\omega, m_q)$ in the transition region. For a determination of the expected order of magnitude of Δ_0, chiral perturbation theory may be used at this point and a rough bound on the slope of $\nu'(\omega, m_q)$ (and thus on Δ_0) can also be obtained a posteriori through a fit of simulation results for the mode number. Whether Δ_0 is in fact negligible with respect to the statistical errors can ultimatly always be checked by varying ϵ at fixed δ.

Run	Lattice	κ	N_{cfg}	aM	$\nu(M, m_{\mathrm{q}})$
D_3	48×24^3	0.13610	160	0.02674	28.6(4)
				0.02377	24.0(4)
				0.02087	19.5(4)
				0.01808	15.2(3)
D_5	48×24^3	0.13625	160	0.02549	26.8(5)
				0.02234	22.6(4)
				0.01923	18.5(4)
				0.01616	14.4(3)
E_4	64×32^3	0.13610	80	0.02674	93.9(12)
				0.02377	78.2(12)
				0.02087	63.4(10)
				0.01808	48.9(9)
E_5	64×32^3	0.13625	80	0.02549	83.2(10)
				0.02234	69.6(9)
				0.01923	56.4(8)
				0.01616	44.6(7)
E_6	64×32^3	0.13635	80	0.02499	78.7(11)
				0.02177	66.6(11)
				0.01856	54.9(9)
				0.01537	43.8(8)

Table 2. Simulation results for the mode number

C   Lattice parameters and simulation results

C.1   Lattice parameters

The numerical studies reported in section 6 are based on representative ensembles of gauge-field configurations for the two-flavour O(a)-improved Wilson theory (cf. subsection 2.2). The ensembles were generated by the authors of ref. [31] and were made available to us through the CLS community effort [32].

In these simulations, the coupling $\beta = 6/g_0^2$ was set to 5.3 in all cases and the sea-quark hopping parameter $\kappa = (8 + 2m_0)^{-1}$ to the values quoted in table 2. The lattice sizes and the numbers N_{cfg} of configurations are also given in the table. The spacing of the two lattices considered was determined to be 0.0784(10) fm [31] and their spatial sizes are thus $L = 1.88(2)$ fm and $L = 2.51(3)$ fm, respectively.

C.2   Computation of the mode number

The mode numbers listed in table 2 were computed stochastically following the lines of section 5. We used the same minmax polynomial of degree $n = 32$ in all cases, with ϵ set to 0.01, and the number N of pseudo-fermion fields was taken to be 1. With these choices, $\delta = 4.4 \times 10^{-4}$, the integral (B.7) evaluates to $M/M_* = 0.96334$ and the approximation error Δ [eq. (5.8)] is estimated to be neglible in our computations.

The statistical errors quoted in table 2 are in the range from 1 to 2 percent. They are practically given by the last term in eq. (5.4), which explains why, with half the statistics on the larger lattices, approximately the same relative accuracy is obtained on all lattices. Moreover, the errors could be further reduced, by a factor 2 at least, by increasing the number N of pseudo-fermion fields.

C.3 O(a)-improvement and renormalization at $\beta = 5.3$

The coefficients of the O(a) counterterms in the quark action [3] and the improved axial current [4] were set to the non-perturbatively determined values $c_{\mathrm{sw}} = 1.90952$ [6] and $c_A = -0.0506$ [33], respectively. We computed the renormalized quark mass via the PCAC relation, using the improved axial current, but neglected the O(am_{q}) corrections in eq. (2.8) since $b_A - b_P = -0.00104(6) \times g_0^2 + \mathrm{O}(g_0^4)$ is very small [35].

Although a different improvement scheme was adopted in ref. [8], it is possible to deduce the one-loop formulae

$$b_\mu = -\frac{1}{2} - 0.111(4) \times g_0^2 + \mathrm{O}(g_0^4), \tag{C.1}$$

$$b_R = -0.031(8) \times g_0^2 + \mathrm{O}(g_0^4), \tag{C.2}$$

from the results published there and in refs. [34, 35]. So far b_μ is only known in perturbation theory and we thus used the one-loop estimate $b_\mu = -0.626$ in eq. (3.11). Noting $am_{\mathrm{c}} = -0.33560(5)$, the subtracted bare mass am_{q} is smaller than 0.01 at all values of κ considered. The calculated O(am_{q}) corrections to M_{R} are therefore at most 0.6% and the corrections to the ratio (7.9) will normally be negligible.

The renormalization factors $Z_A = 0.778(10)$ [36] and $Z_P = 0.543(8)$ [37, 38] needed to pass from the bare masses m and M to the renormalized masses m_{R} and M_{R} in the $\overline{\mathrm{MS}}$ scheme at $2\,\mathrm{GeV}$ have been computed non-perturbatively. As can be seen from table 1, the renormalized sea-quark mass ranges from about 13 to $46\,\mathrm{MeV}$ on the lattices considered. The values of aM in table 2 have, incidentally, been chosen such that $\Lambda_{\mathrm{R}} = (M_{\mathrm{R}}^2 - m_{\mathrm{R}}^2)^{1/2}$ approximately assumes the values $70, 85, 100$ and $115\,\mathrm{MeV}$ at all sea-quark masses.

References

[1] T. Banks and A. Casher, *Chiral symmetry breaking in confining theories*, *Nucl. Phys.* **B 169** (1980) 103 [SPIRES].

[2] K.G. Wilson, *Confinement of quarks*, *Phys. Rev.* **D10** (1974) 2445 [SPIRES].

[3] B. Sheikholeslami and R. Wohlert, *Improved continuum limit lattice action for QCD with Wilson fermions*, *Nucl. Phys.* **B 259** (1985) 572 [SPIRES].

[4] M. Lüscher, S. Sint, R. Sommer and P. Weisz, *Chiral symmetry and O(a) improvement in lattice QCD*, *Nucl. Phys.* **B 478** (1996) 365 [hep-lat/9605038] [SPIRES].

[5] L. Del Debbio, L. Giusti, M. Lüscher, R. Petronzio and N. Tantalo, *Stability of lattice QCD simulations and the thermodynamic limit*, *JHEP* **02** (2006) 011 [hep-lat/0512021] [SPIRES].

[6] ALPHA collaboration, K. Jansen and R. Sommer, *O(a) improvement of lattice QCD with two flavors of Wilson quarks*, *Nucl. Phys.* **B 530** (1998) 185 [*Erratum ibid.* **463** (2002) 517] [`hep-lat/9803017`] [SPIRES].

[7] ALPHA collaboration, R. Frezzotti, P.A. Grassi, S. Sint and P. Weisz, *Lattice QCD with a chirally twisted mass term*, *JHEP* **08** (2001) 058 [`hep-lat/0101001`] [SPIRES].

[8] ALPHA collaboration, R. Frezzotti, S. Sint and P. Weisz, *O(a)-improved twisted-mass lattice QCD*, *JHEP* **07** (2001) 048 [`hep-lat/0104014`] [SPIRES].

[9] L. Giusti, G.C. Rossi and M. Testa, *Topological susceptibility in full QCD with Ginsparg-Wilson fermions*, *Phys. Lett.* **B 587** (2004) 157 [`hep-lat/0402027`] [SPIRES].

[10] M. Lüscher, *Topological effects in QCD and the problem of short-distance singularities*, *Phys. Lett.* **B 593** (2004) 296 [`hep-th/0404034`] [SPIRES].

[11] A.V. Smilga and J. Stern, *On the spectral density of euclidean Dirac operator in QCD*, *Phys. Lett.* **B 318** (1993) 531 [SPIRES].

[12] J.C. Osborn, D. Toublan and J.J.M. Verbaarschot, *From chiral random matrix theory to chiral perturbation theory*, *Nucl. Phys.* **B 540** (1999) 317 [`hep-th/9806110`] [SPIRES].

[13] P.H. Damgaard, J.C. Osborn, D. Toublan and J.J.M. Verbaarschot, *The microscopic spectral density of the QCD Dirac operator*, *Nucl. Phys.* **B 547** (1999) 305 [`hep-th/9811212`] [SPIRES].

[14] C.W. Bernard and M.F.L. Golterman, *Partially quenched gauge theories and an application to staggered fermions*, *Phys. Rev.* **D 49** (1994) 486 [`hep-lat/9306005`] [SPIRES].

[15] S.R. Sharpe and N. Shoresh, *Partially quenched chiral perturbation theory without Φ_0*, *Phys. Rev.* **D64** (2001) 114510 [`hep-lat/0108003`] [SPIRES].

[16] J. Gasser and H. Leutwyler, *Chiral perturbation theory to one loop*, *Ann. Phys.* **158** (1984) 142 [SPIRES].

[17] J. Gasser and H. Leutwyler, *Light quarks at low temperatures*, *Phys. Lett.* **B 184** (1987) 83 [SPIRES]; *Thermodynamics of chiral symmetry*, *Phys. Lett.* **B 188** (1987) 477 [SPIRES]; *Spontaneously broken symmetries: effective lagrangians at finite volume*, *Nucl. Phys.* **B 307** (1988) 763 [SPIRES].

[18] M. Lüscher and F. Palombi, *Fluctuations and reweighting of the quark determinant on large lattices*, `PoS(LATTICE 2008)049`.

[19] L. Giusti, C. Hölbling, M. Lüscher and H. Wittig, *Numerical techniques for lattice QCD in the ϵ-regime*, *Comput. Phys. Commun.* **153** (2003) 31 [`hep-lat/0212012`] [SPIRES].

[20] W.H. Press, S.A. Teukolsky, W.T. Vetterling and B.P. Flannery, *Numerical recipes in FORTRAN*, 2nd edition, Cambridge University Press, Cambridge U.K. (1992).

[21] S.R. Sharpe, *Discretization errors in the spectrum of the hermitian Wilson-Dirac operator*, *Phys. Rev.* **D 74** (2006) 014512 [`hep-lat/0606002`] [SPIRES].

[22] RBC-UKQCD collaboration, C. Allton et al., *Physical results from $2+1$ flavor domain-wall QCD and SU(2) chiral perturbation theory*, *Phys. Rev.* **D78** (2008) 114509 [`arXiv:0804.0473`] [SPIRES].

[23] JLQCD AND TWQCD collaboration, J. Noaki et al., *Convergence of the chiral expansion in two-flavor lattice QCD*, *Phys. Rev. Lett.* **101** (2008) 202004 [`arXiv:0806.0894`] [SPIRES].

[24] ETM collaboration, P. Dimopoulos et al., *Scaling and chiral extrapolation of pion mass and decay constant with maximally twisted mass QCD*, PoS(LATTICE 2008)103.

[25] C.B. Lang, P. Majumdar and W. Ortner, *The condensate for two dynamical chirally-improved quarks in QCD*, *Phys. Lett.* **B 649** (2007) 225 [hep-lat/0611010] [SPIRES].

[26] JLQCD collaboration, H. Fukaya et al., *Two-flavor lattice QCD simulation in the ϵ-regime with exact chiral symmetry*, *Phys. Rev. Lett.* **98** (2007) 172001 [hep-lat/0702003] [SPIRES].

[27] H. Fukaya et al., *Two-flavor lattice QCD in the ϵ-regime and chiral random matrix theory*, *Phys. Rev.* **D76** (2007) 054503 [arXiv:0705.3322] [SPIRES].

[28] P. Hasenfratz et al., *$2 + 1$ Flavor QCD simulated in the ϵ-regime in different topological sectors*, arXiv:0707.0071 [SPIRES].

[29] JLQCD collaboration, H. Fukaya et al., *Lattice study of meson correlators in the ϵ-regime of two-flavor QCD*, *Phys. Rev.* **D77** (2008) 074503 [arXiv:0711.4965] [SPIRES].

[30] J.F. Cornwell, *Group theory in physics. Volume* 3, Academic Press, London U.K. (1989).

[31] L. Del Debbio, L. Giusti, M. Lüscher, R. Petronzio and N. Tantalo, *QCD with light Wilson quarks on fine lattices (I): first experiences and physics results*, *JHEP* **02** (2007) 056 [hep-lat/0610059] [SPIRES].

[32] See https://twiki.cern.ch/twiki/bin/view/CLS/WebHome.

[33] M. Della Morte, R. Hoffmann and R. Sommer, *Non-perturbative improvement of the axial current for dynamical Wilson fermions*, *JHEP* **03** (2005) 029 [hep-lat/0503003] [SPIRES].

[34] M. Lüscher and P. Weisz, *$O(a)$ improvement of the axial current in lattice QCD to one-loop order of perturbation theory*, *Nucl. Phys.* **B 479** (1996) 429 [hep-lat/9606016] [SPIRES].

[35] S. Sint and P. Weisz, *Further results on $O(a)$-improved lattice QCD to one-loop order of perturbation theory*, *Nucl. Phys.* **B 502** (1997) 251 [hep-lat/9704001] [SPIRES]; *Further one loop results in $O(a)$-improved lattice QCD*, *Nucl. Phys. Proc. Suppl.* **63** (1998) 856 [hep-lat/9709096] [SPIRES].

[36] M. Della Morte, R. Sommer and S. Takeda, *On cutoff effects in lattice QCD from short to long distances*, arXiv:0807.1120 [SPIRES].

[37] ALPHA collaboration, M. Della Morte et al., *Non-perturbative quark mass renormalization in two-flavor QCD*, *Nucl. Phys.* **B 729** (2005) 117 [hep-lat/0507035] [SPIRES].

[38] ALPHA collaboration, M. Della Morte et al., *Scaling test of two-flavor $O(a)$-improved lattice QCD*, *JHEP* **07** (2008) 037 [arXiv:0804.3383] [SPIRES].